

# Chapter 7

## Novel Structures of CTAT-DNA Complexes

### 7.1 Introduction

Complexes of DNA with cationic lipids and surfactants have attracted much attention recently due to their potential application as non-viral gene delivery vectors, as well as due to their very interesting electrostatics [1, 2, 3]. Positively charged cationic lipid (CL)-DNA complexes have been found to deliver DNA into cultured cells by electrostatic interaction with the anionic cell membrane. Although the transfection efficiency of these complexes is low, it has several advantages : non-immunogenicity, low toxicity and ease of large scale production.

In this work we address the role of a strongly bound counterion on the formation of cationic surfactant-DNA complexes and their structures. The cationic surfactant used is cetyltrimethylammonium tosylate (CTAT). The counterion in this case is the tosylate ion, which is relatively strongly bound to the surfactant micelles due to its aromatic nature, compared to the much more common  $\text{Cl}^-$  and  $\text{Br}^-$  counterions. In section 7.2 we give a brief introduction to earlier work on lipid-DNA complexes. The experimental techniques used in our studies are described in the section 7.4 and our results in section 7.5. A partial phase diagram of the various structures formed by the complexes as a function of CTAT and DNA concentrations has been determined from x-ray diffraction data. Four different structures have been observed, of which only the intercalated hexagonal has been seen earlier. At low DNA content we find a structure characterized by a two-dimensional square lattice over the whole range of CTAT concentration investigated. At high DNA content we find the intercalated hexagonal structure at low CTAT concentrations and a nematic phase at high

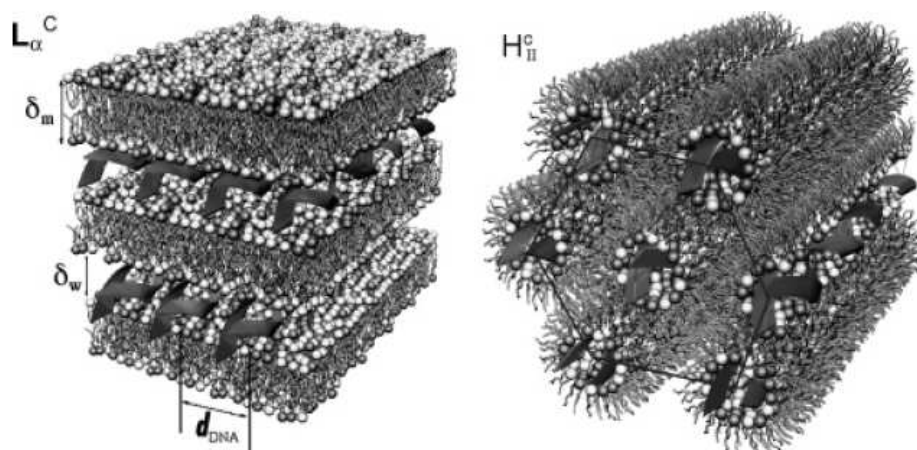


Figure 7.1: Schematic of the intercalated lamellar ( $L_{\alpha}^c$ ) and inverted hexagonal ( $H_{II}^c$ ) phases, most commonly found in cationic lipid-DNA complexes [8].

CTAT content. Another type of complex is seen in between these two, whose structure is yet to be determined. The influence of the salts, NaCl and sodium tosylate (ST), on the structure of these complexes was also studied. In section 7.6 we present models for the electron densities of the intercalated hexagonal and square phases and give some plausible reasons for the occurrence of the different structures in this system. Finally the last section contains the conclusions that can be drawn from the experiments discussed in this chapter.

## 7.2 Earlier studies

Some of the early studies on lipid-DNA complexes suggested a bead-on-string structure, which consists of liposomes connected by the DNA strands [1, 4]. Later on detailed x-ray diffraction studies have been carried out to investigate the structure and morphology of these complexes. Three different structures have been reported in these complexes in water [5, 6, 7, 8]. The intercalated lamellar ( $L_{\alpha}^c$ ) phase is observed with bilayer forming lipids. Here the DNA strands are sandwiched between the lipid bilayers. The DNA form a two-dimensional smectic phase with no long-range positional correlations across the bilayers. However, such correlations can arise below the chain melting transition of the lipid, and the DNA strand form a centred rectangular lattice [9]. The inverted hexagonal ( $H_{II}^c$ ) structure has been found in systems, where the lipids have a tendency to form inverted cylindrical micelles, and also with lipids which form very flexible bilayers (Fig.

7.1). In this phase the lipid-covered DNA strands are arranged on a two dimensional hexagonal lattice. In some systems a transition from  $L_{\alpha}^c$  to  $H_{II}^c$  structure has been observed on heating, and the transition is found to be thermally reversible [10]. The intercalated hexagonal structure ( $H_I^c$ ), where the hexagonally arranged lipid micelles are surrounded by DNA strands, was first observed in complexes of DNA with cationic surfactants that form cylindrical micelles [7].

There have been many investigations on double-chained lipid-DNA complexes, but very few systematic studies on single-chained surfactant-DNA complexes. The latter system has many industrial and biological applications specially for DNA extraction from plants and viruses [11, 12]. There have been some studies to determine the structure of complexes formed by DNA with dodecyltrimethylammonium bromide (DTAB), tetradecyltrimethylammonium bromide (TTAB), and cetyltrimethylammonium bromide (CTAB) with insufficient structural information [13]. A systematic x-ray diffraction study has been recently carried out by Krishnaswamy et. al on CTAB-DNA complexes [7, 14]. These complexes were found to form the  $H_I^c$  phase. However, the  $L_{\alpha}^c$  and  $H_{II}^c$  phases could be induced in this system with the addition of the cosurfactant hexanol.

In aqueous solutions of highly charged polyelectrolytes and ionic surfactants a fraction of the counterions can remain condensed on the macroion, as a result of the competition between electrostatic energy and counterion entropy in minimizing the free energy of the system [15, 16]. This effect depends on the geometry of the macroion, since it determines the distance dependence of the Coulomb energy. It turns out that in the case of a spherical macroion all the counterions are released, whereas in the planar case all of them are condensed on the surface. In the case of linear macroions, both the energy and entropy terms depend logarithmically on the distance from the macroion. Therefore, counterion condensation occurs only if the linear charge density is sufficiently high. The critical value of the separation between charges is set by the Bjerrum length  $l_B$ , which is the distance at which the Coulomb interaction between two elementary charges is equal to the thermal energy  $k_B T$ . If the separation between the charges is less than  $l_B$ , then some of the counterions condense on the macroion, such that the effective separation between the charges becomes  $l_B$ .  $l_B \sim 0.7$  nm in aqueous solutions at 25°C. The average separation between elementary charges along the DNA strand is 0.17 nm. Therefore, a large fraction of the counterions will be

condensed on the DNA, resulting in a reduction in the linear charge density by a factor of 4. A similar effect can be expected in the case of a cylindrical micelle of ionic surfactants, since the typical separation between the molecules is  $\sim 0.45$  nm. Note that the above arguments do not take into account any specific interactions between the counterion and the macroion, which can further enhance the degree of counterion condensation.

When DNA forms a complex with cationic surfactant micelles, the condensed counterions on both the species are released into the solution. The resulting increase in the entropy of these counterions is responsible for the formation of these complexes [17, 18]. The complex usually separates out as a precipitate, whereas the counterions remain in the supernatant solution. The counterion release mechanism of complex formation has been verified experimentally by measuring the counterion concentration in the supernatant [19].

Generally the surfactant aggregate morphology does not change on complexation. However, in some cases, steric effects and the packing properties are found to be dominating factors in determining the morphology [20].

### 7.3 Theoretical phase diagram

A complicated phase behaviour of complexes formed by DNA with mixtures of cationic lipids and co-lipids has been predicted theoretically by taking into account the electrostatic and elastic energies of the system and the mixing entropy of the lipid layers [21, 22].

The major contribution to the electrostatic free energy is the entropy gain due to the release of counterions from both the DNA and lipid molecules. Based on the nonlinear Poisson-Boltzmann (PB) equation, the electrostatic free energy of a charged surface in solution is expressed as,

$$f^{es} = \frac{1}{2} \int_S \sigma \Phi ds + k_B T n_o \int_v [\psi \sinh \psi - 2 \cosh \psi + 2] dv, \quad (7.1)$$

where  $\sigma$  and  $\Phi$  are the local surface charge density and electrostatic potential, respectively.  $\psi = e\Phi/k_b T$  is the reduced electrostatic potential.  $n_o$  is the salt concentration in the solution. The elastic energy density of a lipid monolayer is given by,

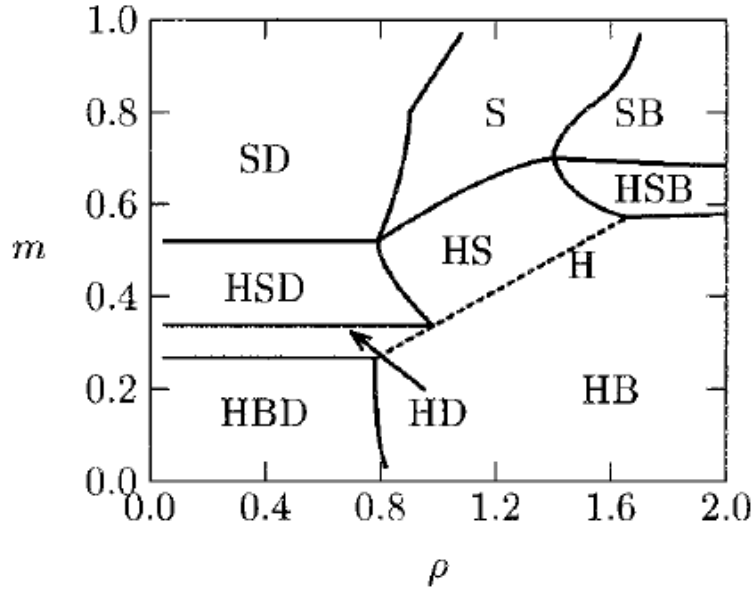


Figure 7.2: The phase diagram of a lipid-DNA mixture, for lipids that self-assemble into very soft planar membranes ( $k = 0$  and  $f_v = 0$ ), calculated as a function of the mole fraction of the cationic lipid,  $m$ , and the lipid to DNA charge ratio  $\rho$ . S, B, H and D denote the  $L_\alpha^c$ ,  $L_\alpha$ ,  $H_{II}^c$  and uncomplexed DNA phases, respectively [21].

$$f^{el} = A \frac{k}{2} (c - c_o)^2 + f_v \quad (7.2)$$

where  $k$  is the bending modulus of the lipid layer,  $c$  and  $c_o$  the actual and spontaneous curvatures and  $A$  the area per molecule. The first term is the deformation energy per molecule in a cylindrically bent lipid layer.  $f_v$  arises from the average stretching per molecule which vanishes in the  $L_\alpha$  and  $L_\alpha^c$  phases but is non-zero in the inverted phase. The mixing free energy of the monolayer in different phases is given by,

$$f^{mix}/k_B T = \phi \ln \phi + (1 - \phi) \ln(1 - \phi) \quad (7.3)$$

where  $\phi$  is the lipid composition.

Minimizing the total free energy with respect to the relevant variables, the phase diagram has been calculated in the  $\rho$  (lipid/DNA ratio) -  $m$  (mole fraction of cationic lipid in the lipid mixture) plane. A typical phase diagram is shown in figure 7.2, where the existence of the  $L_\alpha^c$  and  $H_{II}^c$  structures are predicted.

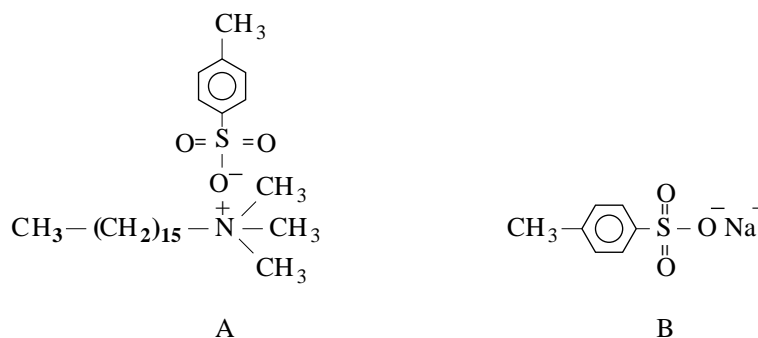


Figure 7.3: Chemical structure of : (A) cetyltrimethylammonium tosylate (CTAT) and (B) sodium *p*-toluene sulfonate (ST).

## 7.4 Experimental

Cetyltrimethylammonium tosylate (CTAT) and sodium salt of “highly polymerized” calf thymus DNA were obtained from Sigma. The chemicals were used as received. Their structures are shown in figure 7.3. The concentration of CTAT solution ( $C_s$ ) was varied from 10mM to 250mM. The solution was prepared with deionized water (Millipore). Measured amounts of DNA fibre were added to this solution. For each value of  $C_s$ ,  $\rho$  [= (wt. of CTAT)/(wt. of DNA)] was varied over a wide range about the isoelectric point ( $\rho_{iso} = 1.41$ ), where the number of surfactant molecules is equal to the number of DNA bases. To check the effect of salts, stock solutions of NaCl and sodium *p*-toluene sulfonate (ST) were prepared. Measured amount of CTAT and DNA fibre were added to it. The complex was collected in 1mm diameter glass capillary for x-ray diffraction experiments, the details of which have been given in previous chapters.

IR absorption spectra were recorded with a *Shimadzu FTIR-8400* spectrometer keeping the sample in AgCl cell (*Thermo Electron Corporation*). UV absorption spectra were recorded with a *Hitachi U3200* spectrometer taking the sample in quartz cell. The supernatant was collected after centrifugation at a speed of 4000 rpm for 20 minutes.

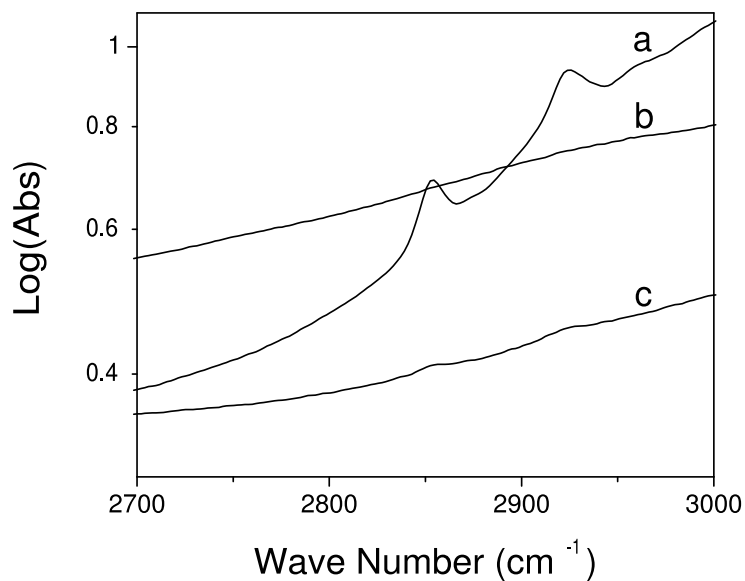


Figure 7.4: IR spectra of (a) CTAT solution at  $C_s = 100\text{mM}$  and  $\rho = \infty$ , (b) CTAT-DNA supernatant at  $C_s = 100\text{mM}$  and  $\rho = 0.38$  and (c) CTAT-DNA supernatant at  $C_s = 100\text{mM}$  and  $\rho = 4.2$ .

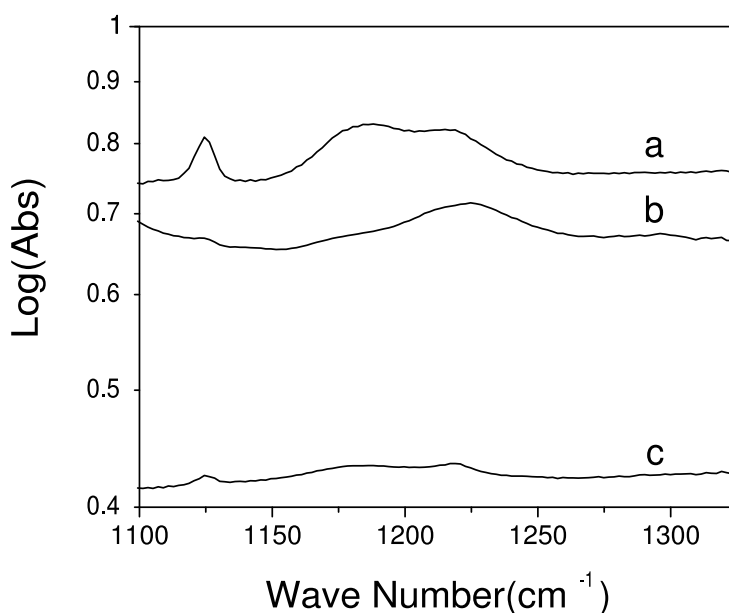


Figure 7.5: IR spectra of (a) CTAT solutions at  $C_s = 100\text{mM}$  and  $\rho = \infty$  (b) CTAT-DNA supernatant for  $\rho < \rho_{iso}$  at  $C_s = 100\text{mM}$  and  $\rho = 0.38$  (c) CTAT-DNA supernatant for  $\rho > \rho_{iso}$  at  $C_s = 100\text{mM}$  and  $\rho = 4.2$ . All the three compositions show the existence of tosylate counterions into the supernatant.

## 7.5 Results

### 7.5.1 Formation of complex

As discussed earlier, the formation of the complex is driven by the entropy gain due to the release of the counterions both from the surfactant and the polyelectrolyte [19]. CTAT surfactant has the *p*-toluene sulfonate (also known as tosylate) counterion, which binds much more strongly to the micelle, compared to  $\text{Cl}^-$  and  $\text{Br}^-$  ions, due to its aromatic nature. NMR studies on similar systems have shown that these counterions sit on the micellar surface with their hydrophobic part immersed in the hydrocarbon region of the micelle. Although the tosylate ion is soluble in water, it is, therefore, not clear if the majority of the counterions are released into the solvent on complexation. In order to check this, IR spectroscopy studies of the supernatant of the complex were performed. For pure CTAT solutions ( $\rho = \infty$ ) we find the characteristic absorption due to C-H stretching at 2854.5 and 2925  $\text{cm}^{-1}$ . These are also seen in the supernatant for  $\rho > \rho_{iso}$ , coming from the uncomplexed CTAT molecules. For  $\rho < \rho_{iso}$ , these absorption peaks are not seen ( Fig. 7.4), since at these compositions all the CTAT molecules are incorporated in the complex. There are a number of additional absorption peaks at around 1250 to 1100  $\text{cm}^{-1}$  arising from the tosylate counterions. All the three compositions ( $\rho = \infty$ ,  $\rho > \rho_{iso}$  and  $\rho < \rho_{iso}$ ) show these peaks indicating the presence of released counterions in the supernatant ( Fig 7.5). Ratio of the areas under the tosylate and C-H absorption peaks is found to be four times higher for CTAT-DNA complex at  $C_s = 100\text{mM}$  and  $\rho = 4.2$  compared to pure CTAT solutions at 100mM. It indicates the existence of extra counterions in the supernatant, which are released due to the formation of the complex.

The presence of uncomplexed DNA was verified using UV-spectroscopy of the supernatant of the complex at  $\rho < \rho_{iso}$ . Under these conditions a strong absorption peak is observed at around 260nm which is a characteristic peak of the DNA molecule. This peak is not found at  $\rho > \rho_{iso}$  (Fig. 7.6).



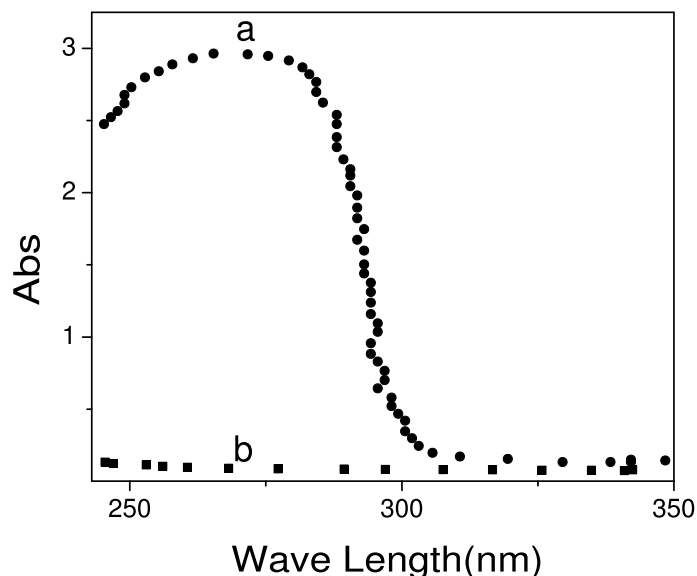


Figure 7.6: UV spectra of (a) CTAT-DNA supernatant for  $\rho < \rho_{iso}$  at  $C_s = 50\text{mM}$  and  $\rho = 0.7$ , (b) CTAT-DNA supernatant for  $\rho > \rho_{iso}$  at  $C_s = 50\text{mM}$  and  $\rho = 4.0$ .

### 7.5.2 Structure of complex

DNA-CTAT complexes at all compositions show birefringence under a polarizing microscope indicating the formation of anisotropic phases. X-ray diffraction studies show three different diffraction patterns indicating different structures depending on surfactant and DNA concentrations (Fig. 7.7). The phase diagram of the system determined from the diffraction data is shown in figure 7.8.

At low surfactant concentrations and high DNA content the diffraction pattern shows three peaks with their  $q$  values in the ratio  $1:\sqrt{3}:2$  corresponding to  $(1\ 0)$ ,  $(1\ 1)$  and  $(2\ 0)$  reflections from a 2-D hexagonal lattice. With increasing CTAT concentration ( $C_s$ ), the lattice parameter  $a$  is found to increase whereas it is independent of  $\rho$ .  $a$  increases by around  $10\text{\AA}$ , from  $C_s = 10\text{ mM}$  to  $75\text{ mM}$  ( Table 7.1).

At low values of  $C_s$  the hexagonal structure transforms to a different structure on decreasing the amount of DNA (Fig. 7.8). X-ray data from this phase could be indexed on a square lattice as shown in table 7.2. From the shape of the phase boundary it is clear that the amount of DNA required to have this hexagonal to square transition increases with increasing surfactant concentration. For  $C_s < 150$ , the lattice parameter of the square phase is almost independent of both surfactant and DNA concentrations. A slight increase is observed at higher  $C_s$  (Table 7.3). This

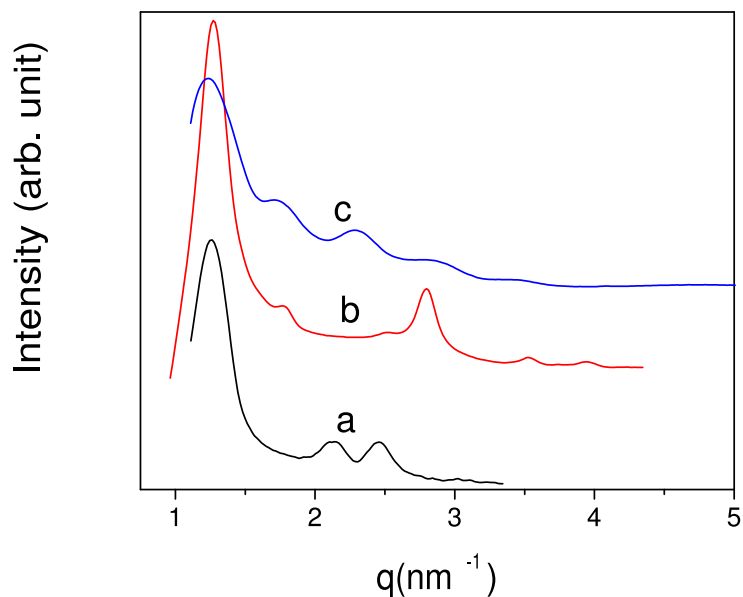


Figure 7.7: Diffraction patterns of the different phases: (a) hexagonal at  $C_s = 50\text{mM}$  and  $\rho = 0.7$ , (b) square at  $C_s = 75\text{mM}$  and  $\rho = 4.16$  and (c) rectangular at  $C_s = 100\text{mM}$  and  $\rho = 1.41$ .

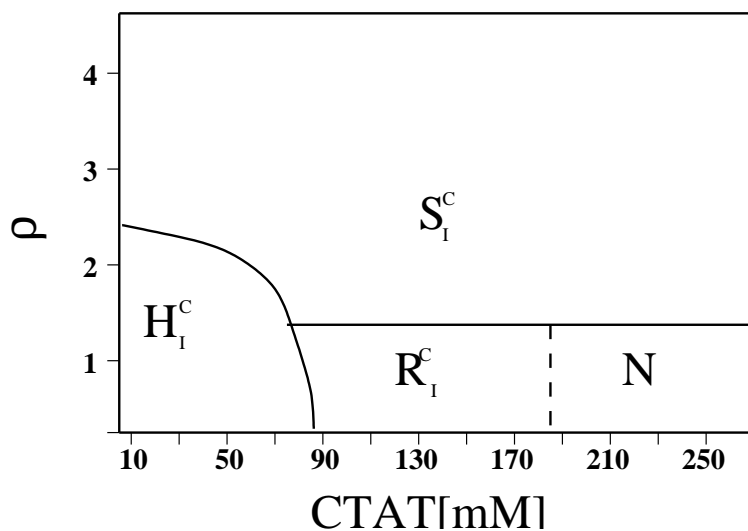


Figure 7.8: Partial phase diagram of DNA-CTAT complexes showing hexagonal ( $H_I^c$ ), square ( $S_I^c$ ) and rectangular ( $R_I^c$ ) phases. N indicates the nematic phase which appears at very high surfactant concentrations in the presence of high amount of DNA.

Table 7.1: Variation of the lattice parameter  $a$  of the hexagonal phase with surfactant concentration ( $C_s$ ) and with CTAT to DNA weight ratio ( $\rho$ ).

$C_s$ (mM)	$\rho$	$a$ (nm)
10	0.70	5.19
	1.41	5.17
50	0.70	5.74
	1.41	5.79
	2.0	5.79
75	0.5	6.02
	0.98	6.06

Table 7.2: Indexing of x-ray diffraction data on a square lattice for the DNA-CTAT complex at  $C_s = 75$ mM and  $\rho = 1.41$ .

$d_{exp}$ (nm)	$d_{calc}$ (nm)	Plane	Intensity
4.95	4.95	(10)	vvs
3.53	3.50	(11)	w
2.50	2.47	(20)	w
2.23	2.21	(12)	vs
1.78	1.75	(22)	vw
1.59	1.56	(13)	vw

phase is observed over the whole range of surfactant concentration studied at high values of  $\rho$  (low DNA content).

At much higher values of CTAT concentration ( $C_s > 90$ mM) with high DNA content, another kind of diffraction pattern is observed for low values of  $\rho$ . These data can be indexed on a simple rectangular lattice (Table 7.4). The transition from the square to this phase with the addition of DNA has been clearly observed in the experimental data with gradual appearance of extra peaks (Fig. 7.9). One of the lattice parameters,  $a$  changes to slightly lower values with decreasing DNA content but the other one  $b$  remains almost same (Table 7.5). With further increase in the surfactant concentration at high DNA content, another structure is found, which gives a diffuse x-ray diffraction peak (Fig. 7.10). This is a characteristic pattern of the nematic phase where the

Table 7.3: Variation of the lattice parameter  $a$  of the square phase with surfactant concentration ( $C_s$ ) and with CTAT to DNA weight ratio ( $\rho$ ).

$C_s$ (mM)	$\rho$	$a$ (nm)
10	2.82	5.01
	5.37	5.03
50	2.2	5.09
	4.2	4.94
75	1.41	4.95
	4.16	4.95
90	1.92	5.03
	4.03	4.95
150	1.43	5.21
	4.38	5.00
200	2.05	5.40
	4.54	5.23
250	2.24	5.30
	4.03	5.30

long-range positional order of the lattice is lost, and only long-range orientational order is retained. The diffuse peak appears at around 6.5nm which decreases slightly with increasing  $C_s$ . Such a length scale is not expected from an ordered structure formed by concentrated DNA solution. Consistent with this, no diffraction peak is observed from the supernatant at these compositions, which contains the excess DNA. It should be mentioned that there is no effect of temperature on the structure of different phases in this system. The temperature was varied from 30 °C to 75 °C.

### 7.5.3 Stability of complex: Effect of salt

As mentioned earlier, in the present system the dissociated surfactant counterion has special affinity to get adsorbed on the surfactant micelles. To check the influence of the degree of absorption of counterions in determining the structure of complex, changes in the structure of the complex induced by different salts were investigated. Simple inorganic salt NaCl was added to the hexagonal phase at the composition  $C_s = 10 \text{ mM}$  and  $\rho \sim 0.71$ . The lattice parameter of this phase is found to

Table 7.4: Indexing of x-ray diffraction data on a simple rectangular lattice for the DNA-CTAT complex at  $C_s = 100\text{mM}$  and  $\rho = 0.387$ .

$d_{exp}(\text{nm})$	$d_{calc}(\text{nm})$	Plane	Intensity
5.68	5.68	(10)	vvs
4.78	4.78	(01)	s
3.66	3.65	(11)	s
2.84	2.84	(20)	w
2.20	2.20	(12)	vw

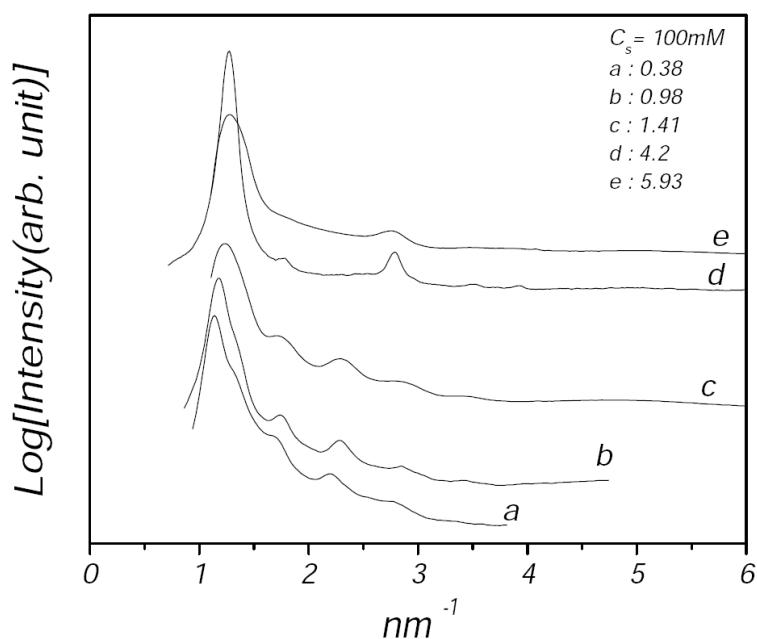


Figure 7.9: Variation of the diffraction patterns across the rectangle to square transition at  $C_s = 100\text{mM}$ . Values of  $\rho$  are (a) 0.38, (b) 0.98, (c) 1.41, (d) 4.2 and (e) 5.93. Patterns a to c correspond to the rectangular phase, and d,e to the square phase.

Table 7.5: Variation of the lattice parameters of the rectangular phase with surfactant concentration ( $C_s$ ) and with CTAT to DNA weight ratio ( $\rho$ ).

$C_s(mM)$	$\rho$	$a$	$b$
90	1.31	5.25	4.8
100	0.38	5.68	4.78
	0.725	5.65	-
	0.97	5.35	4.79
	1.41	5.31	4.84
150	0.99	5.38	4.76

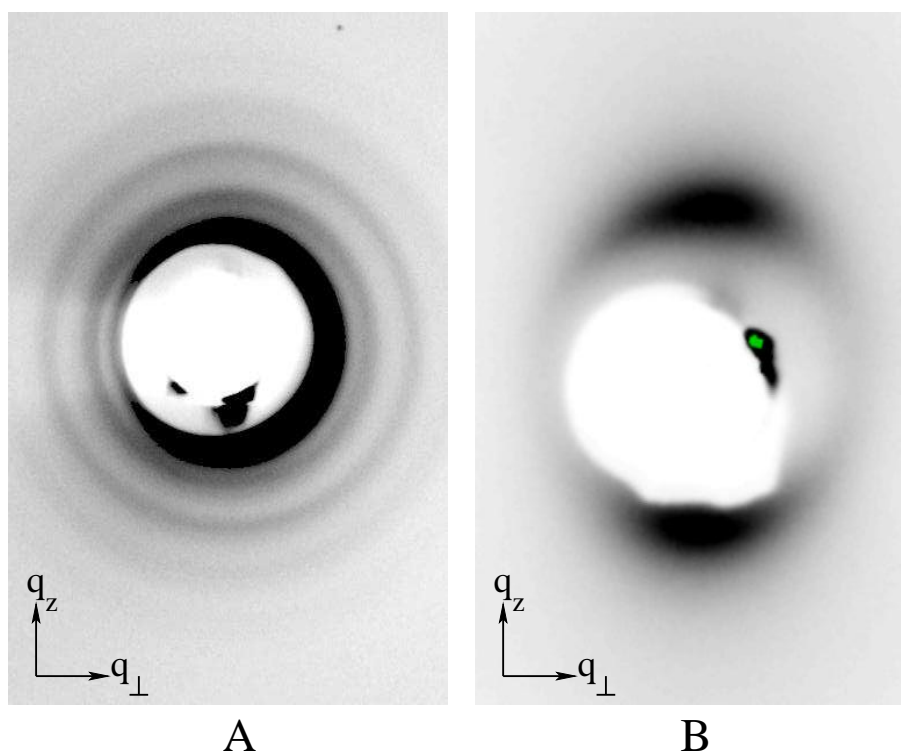


Figure 7.10: Diffraction patterns of the CTAT-DNA complexes at  $\rho = 1.41$  for (A)  $C_s = 100mM$  and (B)  $250mM$ . It shows the melting of an ordered structure on increasing the concentration of the surfactant solution.

Table 7.6: Effect of NaCl on the structure of different phases in CTAT-DNA system at  $C_s = 10$  mM. ID denotes ‘isotropic dispersion’.

$\rho$	NaCl(mM)	phase	$a$
0.71	0	hexagonal	5.25
	75	hexagonal	5.68
	250	hexagonal	5.77
	500	hexagonal	6.06
	750	ID	-
4.2	0	square	5.01
	75	square	5.02
	250	square	5.01
	500	square	5.02
	750	ID	-

increase with increasing NaCl concentration (Table 7.6). However, the addition of NaCl is not able to change the structure of the complex. At very high salt concentration, the complex melts into an isotropic dispersion. NaCl was also added to the square phase at  $C_s = 10$  mM and  $\rho \sim 4.20$  and it had no effect on the lattice parameter of this phase. However, as in the previous case an isotropic dispersion is formed at very high salt concentration. The critical salt concentration to form the isotropic dispersion is similar for both phases. The swelling of the hexagonal phase seems to be a general feature and does not depend upon the type of surfactant, as it is observed on the addition of NaBr to the cetyltrimethylammonium bromide (CTAB)-DNA complex. In this case the lattice parameter has been found to increase from 5.12 to 6.43nm and then the complex dissolves into an isotropic dispersion at around 500mM of salt.

The behaviour is completely different when sodium *p*-toluene sulfonate (ST) is added to the complex. As in the case of NaCl, this salt was also added to the hexagonal and square phases. The hexagonal phase at  $C_s = 10$  mM and  $\rho \sim 0.71$  is found to initially swell and then transform to the rectangular and square phases with progressive addition of ST. At high salt concentration an isotropic dispersion is again formed. Interestingly, when the salt was added to the hexagonal phase at  $C_s = 10$  mM and  $\rho \sim 1.41$ , this phase first swells and then it transforms to the square phase. Both

Table 7.7: Effect of sodium *p*-toluene sulfonate (ST) on the structure of different phases in the CTAT-DNA system at  $C_s = 10 \text{ mM}$ . ID denotes ‘isotropic dispersion’.

$\rho$	$ST(mM)$	<i>phase</i>	<i>a</i>
0.71	0	hexagonal	5.25
	50	rectangular	5.25,4.58
	75	square	5.25
	100	ID	-
1.41	0	hexagonal	5.07
	40	hexagonal	6.01
	90	square	5.36
	100	ID	-
4.2	0	square	5.01
	40	square	5.24
	90	square	5.24
	100	ID	-

observations at  $\rho \sim 0.71$  and 1.41 are consistent with the phase boundary in the phase diagram of the complexes without any added salt. ST was also added to the square phase at  $C_s = 10$  and  $\rho \sim 4.2$ . Unlike the other phases the square phase does not show any change in its structure but only a very small change in the lattice parameter (Table 7.7). The effect of ST is found to be much more pronounced than that of NaCl, as manifested by the much lower critical salt concentration needed to induce the isotropic dispersion (Table 7.6 & 7.7).

## 7.6 Discussion

### 7.6.1 Formation of the complex

NMR studies show that counterions such as tosylate like to sit near the surface of the surfactant micelle inserting their aromatic ring into the micelles [23, 24]. Unlike other systems studied earlier, with simpler counterions such as  $\text{Cl}^-$  and  $\text{Br}^-$ , in the present system it is in principle possible that the released counterions are retained in the micelle. IR spectroscopy results indicate that the amount of tosylate counterion is much more in the supernatant of the complex compared to



the CTAT solution of same total surfactant concentration. Therefore, release of counterions on complexation is taking place even in this system, and must be the driving force for complexation as in other systems studied earlier.

Results of UV spectroscopy studies support the presence of uncomplexed DNA in the supernatant when  $\rho < \rho_{iso}$ . For  $\rho > \rho_{iso}$ , all the DNA are utilized to form the complex. In such a situation the supernatant is found to contain only the surfactant. On either sides of the isoelectric point the supernatant contains the excess component, as in the case of systems with simpler counterions.

### 7.6.2 Modelling of structures

The hexagonal phase ( $H_7^c$ ) seen in this system is similar to the one seen in CTAB-DNA complexes. The scattering from this phase has been analysed in detail by Krishnaswamy et al [14], and shown to be consistent with an intercalated structure. In this structure each DNA strand is intercalated between three micelles (Fig. 7.11A). From this close packed micelle-DNA structure, the cylinder radius of CTAT micelles was estimated and is found to increase from 1.75 nm at  $C_s = 10\text{mM}$  to 2.1nm at  $C_s = 50\text{mM}$ . Such an increase of micellar radius with surfactant concentration has also been reported in other systems [25].

The main result of this work is the observation of three new kinds of non-lamellar assemblies of surfactant and DNA molecules. The square, rectangular and nematic phases of these complexes have not been reported until now. The lattice parameter of the square phase ( $S_7^c$ ) is consistent with a closed-packed structure, where each micelle is surrounded by four DNA strands (Fig. 7.11B). For example, at  $C_s = 50\text{mM}$  and  $\rho = 1.41$ , the experimental value of  $a$  is 4.9 nm, whereas the calculated value is 4.8 nm. In this structure there is one DNA strand per micelle. On the other hand, in the hexagonal phase there are two DNA strands per micelle. This is consistent with the observation that the square structure is obtained from the hexagonal phase on decreasing the DNA content. We have carried out detailed analysis of the diffraction data to check the proposed structure. We model the two dimensional electron density of the square structure and compare the calculated relative intensities with those observed. The details of such an analysis for the hexagonal phase has been described elsewhere [14].

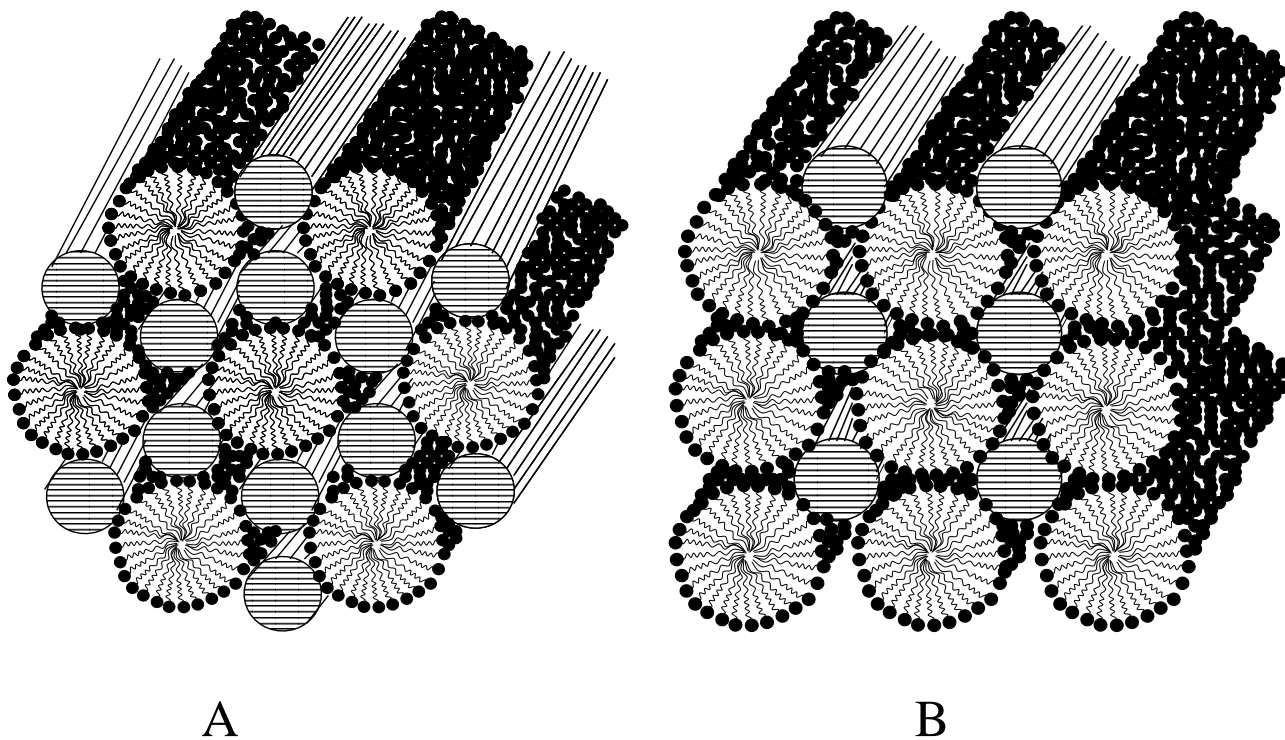


Figure 7.11: The schematic diagrams of (A) hexagonal and (B) square phases of CTAT-DNA complexes.

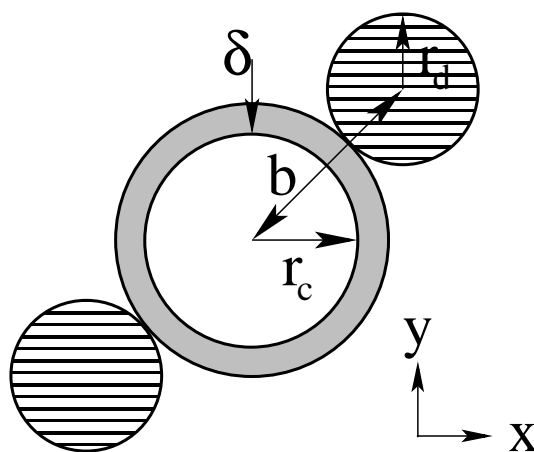


Figure 7.12: The electron density model used to calculate the diffraction data of the  $S_I^c$  phase. The disc with radius  $r_c$  represents the hydrocarbon region of the micelles. The shaded annular ring of thickness  $\delta$  corresponds to the head group region. The other shaded disc with radius  $r_d$  is the DNA.

The electron density of the structure can be written as,

$$\rho_c(\vec{r}) = \rho_l(\vec{r}) \otimes \rho(\vec{r}), \quad (7.4)$$

where  $\rho_l(\vec{r})$  is the lattice function describing the square lattice and  $\rho(\vec{r})$  is the basis function describing the contents of a unit cell.  $\otimes$  denotes convolution of the two functions. Fourier transform of this relation gives,

$$F(\vec{q}) = f_l(\vec{q}) \times f(\vec{q}), \quad (7.5)$$

The intensity of the scattered radiation is given by,

$$I(\vec{q}) = |F(\vec{q})|^2 \quad (7.6)$$

We consider a symmetric basis to make the calculation simpler (Fig. 7.12). The space in between the micelles and DNA is filled with water.  $\rho_c$  is the uniform electron density of the hydrocarbon region of the micelle which is modelled as a disk of radius  $r_c$ .  $\delta$  is the thickness of the annular ring of the head group region with electron density  $\rho_h$ . The disk with radius  $r_d$  is the hydrated DNA strand with electron density  $\rho_d$ . The values of  $\rho_c$  and water electron density  $\rho_w$  are taken as  $280 \text{ e/nm}^3$  and  $332 \text{ e/nm}^3$  [26]. The value of  $r_d$  is well known to be 1.25 nm. The radius of cylindrical micelle is calculated to be 2.1 nm. The value of  $r_c$  is then defined as  $(2.1-\delta)\text{nm}$ . The value of  $\rho_d$  is taken from [14] to be  $400 \text{ e/nm}^3$ . We take  $\rho_h$  and  $\delta$  to be adjustable parameters in our model since on complexation they can take up different values. The electron density of the unit cell is the convolution of the electron density of a DNA cylinder  $\rho_{dna}(r)$  with a set of delta functions representing their positions, plus the electron density of the micelle  $\rho_m(r)$ . We take a factor of half in front of the electron density of DNA since the unit cell effectively has only one DNA strand.

$$\rho^{Si}(\vec{r}) = \frac{1}{2}\rho_{dna}(r) \otimes \delta(r - b)\{\delta(\theta - \pi/4) + \delta(\theta + 3\pi/4)\} + \rho_m(r), \quad (7.7)$$

where  $\theta$  is the angle made by the position vector  $\vec{r}$  with the x-axis, and  $b (= r_c + \delta + r_b)$  is the distance between centres of the micelle and the DNA strand. The electron density of DNA is given

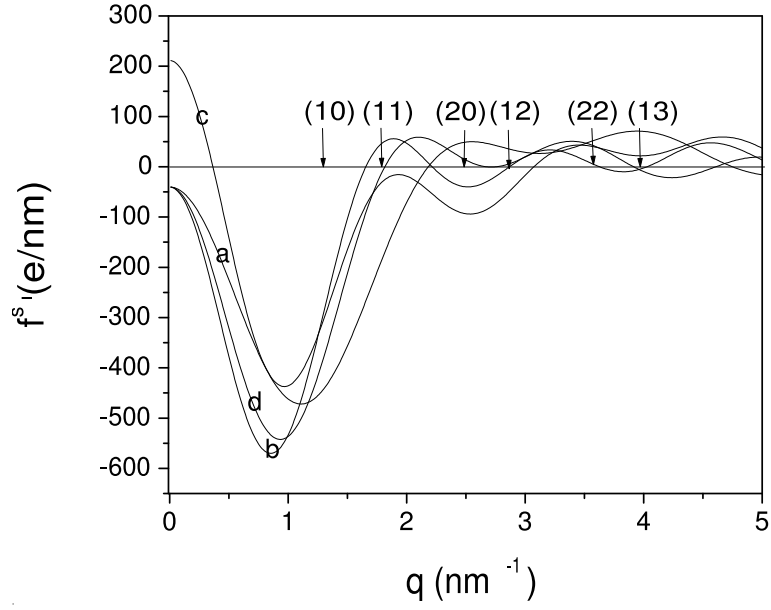


Figure 7.13: Variation of the form factor of the  $S_I^c$  structure along (a)  $\hat{q}_{10}$ , (b)  $\hat{q}_{11}$ , (c)  $\hat{q}_{12}$  and (d)  $\hat{q}_{13}$  for  $a = 4.95\text{nm}$ ,  $\rho_h = 325 \text{ e/nm}^3$  and  $\delta = 0.7 \text{ nm}$ . The values of the other parameters are discussed in the text. The arrows show the positions of the observed peaks.

by,

$$\rho_{dna}(r) = \rho_d - \rho_w, r < r_d \quad (7.8)$$

$$= 0, r > r_c + \delta \quad (7.9)$$

The electron density of the micelle is given by,

$$\rho_m(r) = \rho_c - \rho_w, r < r_c \quad (7.10)$$

$$= \rho_h - \rho_w, r_c < r < r_c + \delta \quad (7.11)$$

$$= 0, r > r_c + \delta \quad (7.12)$$

To get the form factor of the square structure ( $S_I^c$ ), we take the Fourier transform of equation (7.7) using the above expressions for  $\rho_m$  and  $\rho_{dna}$ ,

Table 7.8: Comparison of experimental ( $I_{exp}$ ) and calculated ( $I_{calc}$ ) intensities of the square phase at  $C_s = 75\text{mM}$  and  $\rho = 4.16$ . The best fit values of the parameters  $\rho_h$  and  $\delta$  are  $325\text{e}/\text{nm}^3$  and  $0.7\text{nm}$ , respectively.

$(hkl)$	$I_{exp}$	$I_{calc}$
(10)	100	100
(11)	1.73	1.12
(20)	1.62	0.67
(12)	3.74	3.17
(22)	0.12	0.10
(13)	0.08	0.17

$$f^{S_c}(q, \phi) = 2\pi \cos\left\{\frac{qb}{\sqrt{2}}(\cos\phi + \sin\phi)\right\} r_d J_1(qr_d)/q + f_m(q), \quad (7.13)$$

where  $\phi$  is the angle between the reciprocal lattice vector  $\vec{q}$  and the x-axis.  $J_1(x)$  is the Bessel function of order 1.  $f_m(q)$  is the Fourier transform of  $\rho_m(q)$  which is given by,

$$f_m(q) = 2\pi(\rho_h - \rho_w)r_h J_1(qr_h)/q - 2\pi(\rho_h - \rho_c)r_c J_1(qr_c)/q, \quad (7.14)$$

where  $r_h = r_c + \delta$ . The variation of the form factor in different directions is shown in figure 7.13. The calculated relative intensities along with the experimental values are shown in table 7.8. The experimental values are multiplied by corresponding  $q$  values of the peaks to take care of the unoriented nature of the sample. The multiplicity factor of (12) and (13) reflections are twice that of the other reflections. Hence the intensities of (12) and (13) are reduced by a factor of 2. The electron density of head group of the surfactant and its thickness are found to be  $325\text{e}/\text{nm}^3$  and  $0.7\text{nm}$ , respectively, from the best fit between the calculated and observed intensities. These values are found to be comparable to those reported in the literature [27]. The intercalated structure of the square phase is thus consistent with the diffraction data.

The observation of the rectangular phase in between the hexagonal and square on adding ST suggests an intermediate structure of this phase. Diffraction data from this phase could be indexed on a simple rectangular lattice, but the arrangement of the micelles and DNA within such a lattice is

not clear. One possibility is that the cross-section of the cylindrical micelles changes from circular in the square phase to elliptical in the rectangular phase. However, it is not apparent why such a structure would appear between the square and hexagonal phases, both of which have micelles with circular cross-section. Further, we were not able to induce such ‘ribbon-like’ micelles in the CTAT-water system by adding ST. Higher resolution data are clearly needed to determine the structure of this phase.

The occurrence of a nematic phase at high surfactant concentration is consistent with the gradual melting of the complex in the presence of increasing amounts of salt. However, this phase is not observed when ST is added either to the hexagonal or square phases. In both these cases, only a slightly turbid isotropic dispersion of small non-birefringent aggregates is obtained. With further addition of salt even these aggregates disappear and a clear solution is obtained. These observations, together with the fact that the nematic phase is seen only at high DNA content suggests that this phase is stabilized by the osmotic pressure due to the excess DNA in the supernatant. The average separation of  $\sim 6.5$  nm seen in this phase is comparable to the sum of the radii of the CTAT micelle and DNA. This suggests that the local arrangement of the micelles and DNA in this phase is somewhat similar to those in the other phases, but with no long range positional correlations.

### **7.6.3 Phase transitions**

The observation of various phases with increasing surfactant concentration ( $C_s$ ) is a novel feature of the present work. Earlier studies on similar systems show the structure of the complex to be independent of the surfactant concentration [28]. In all these systems, increasing  $C_s$  and DNA content increases the dissociated salt which plays an important role in determining the stability of the complex. Addition of simple inorganic salts to cationic lipid-DNA complexes destabilizes the lamellar complex formed in these systems [29]. Interestingly these salts are not able to induce any other ordered phases in these complexes. On the other hand, the tosylate counterion released by the CTAT molecules on complexation has a tendency to bind strongly to the micelle. Thus in the present system there is a competition between the tosylate counterions and the phosphate ions on the DNA to bind to the micelle. At low DNA concentration, all the DNA molecules bind to

the micelles with a minimal release of tosylate counterion to give rise to the square phase. At higher DNA concentration, more DNA bind to the micelles at the expense of tosylate to give rise to the hexagonal phase. From square to hexagonal phase, the number of DNA molecules to each micelle in the unit cell increases from one to two. This explanation is consistent with observations on adding ST to the hexagonal phase. The rectangular phase found in between the hexagonal and square should have an intermediate structure which is yet to be determined. The appearance of the nematic phase is the consequence of melting of ordered structure due to the dissociated salt. Similar melting of ordered structures on lowering the water content has been seen in other charged polyelectrolyte systems, again due to the released counterions [30].

## **7.7 Conclusion**

We have studied surfactant-DNA complex formation in a system with strongly bound counterions. The basic ‘counterion release’ mechanism is found to hold good in this system as in other systems with simpler counterions. Novel phases and transitions between them have been observed due to the competition between the counterion and the DNA to bind to the micelles. Along with the intercalated hexagonal phase, reported earlier, the square and the rectangular phases have been seen where the surfactant cylinders are surrounded by DNA stands giving rise to intercalated structures. The x-ray diffraction data from the square phase has been analyzed in detail to substantiate the proposed structure. Further experiments are required to deduce the exact structure of the rectangular phase. The phase transitions are found to be driven by the presence of strongly bound counterions, as verified by directly adding ST to the complex; these transitions are not seen when NaCl is added instead. The complex is found to melt at high surfactant concentrations to form a positionally disordered but orientationally ordered nematic phase.

# Bibliography

- [1] P. L. Felgner, T. R. Gadek, M. Holm, R. Roman, H. W. Chan, M. Wenz, J. Northrop, G. M. Ringold and M. Danielsen *Proc. Natl. Acad. Sci., U. S. A.*, **84**, 7413 (1987).
- [2] P. Bruni, M. Pisani, A. Amici, C. Marchini, M. Montani and O. Francescangell *Appl. Phys. Lett.*, **88**, 073901 (2006).
- [3] G. Caracciolo, C. Marchini, D. Pozzi, R. Caminiti, H. Amenitsch, M. Montani and A. Amici *Langmuir*, **23**, 4498 (2007).
- [4] P. L. Felgner and G. Rhodes *Nature*, **349**, 351(1991).
- [5] J. O. Radler, I. Koltover, T. Saldittand and C. R. Safinya *Science*, **275**, 810 (1997).
- [6] I. Koltover, T. Saldittand, J. O. Radler and C. R. Safinya *Science*, **281**, 78 (1998).
- [7] R. Krishnaswamy, V. A. Raghunathan and A. K. Sood *Phys. Rev. E*, **69**, 031905 (2004).
- [8] K. K. Ewert, H. M. Evans, A. Zidovska, N. F. Boussein, A. Ahmed and C. R. Safinya *J. Am. Chem. Soc.*, **128**, 3998 (2006).
- [9] A. Artzner, R. Zantl, G. Rapp, and J. O. Radler *Phys. Rev. Lett.*, **81**, 5015 (1998).
- [10] W. L. Hsu, Y. C. Li, H. L. Chen, W. Liou, U. S. Jeng, H. K. Lin, W. L. Liu and C. S. Hsu *Langmuir*, **22**, 7521 (2006).
- [11] N. Stein, G. Herren and B. Keller *Plant Breeding*, **120**, 354 (2001).
- [12] G. Manfioletti and C. Schneider *Nucleic Acids Research*, **16**, 2873 (1988).



- [13] R. Ghirlando, E. J. Watchtel, T. Arad and A. Minsky *Biochemistry*, **31**, 7110 (1992).
- [14] R. Krishnaswamy, G. Pabst, M. Rappolt, V. A. Raghunathan and A. K. Soodn *Phys. Rev. E*, **73**, 031904 (2006).
- [15] F. Oosawa *Biopolymers*, **6**, 1633 (1968).
- [16] G. S. Manning *J. Chem. Phys.*, **51**, 924 (1969).
- [17] F. Oosawa *J. Polym. Sci*, **236**, 421 (1957).
- [18] R. Bruinsma *Euro Phys. J. B* **4**, 75 (1998).
- [19] K. Wagner, D. Harries, S. May, V. Kahl, J. O. Radler and A. Ben-Shaul *Langmuir*, **16**, 303 (2000).
- [20] G. Caracciolo, D. Pozzi and R. Caminitti *Appl. Phys. Lett*, **89**, 043901 (2006).
- [21] S. May, D. Harries and A. Ben-shaul *Biophys. J.*, **78**, 1681 (2000).
- [22] D. Harries, S. May, W. M. Gelbart, and A. Ben-shaul *Biophys. J.*, **75**, 159 (1998).
- [23] P. A. Hassan, S. R. Raghavan and E. W. Kaler *Langmuir*, **18**, 2543 (2002).
- [24] B. K. Mishra, S. D. Samant, P. Pradhan, S. B. Mishra and C. Manohar *Langmuir*, **9**, 894 (1993).
- [25] F. Husson, H. Mustacchi and V. Luzzati *Acta Cryst.*, **13**, 668 (1960).
- [26] B. Cabane in *Surfactant Solutions: New Methods of Investigation*, Ed. R. Zana, Marcel Dekker, New York (1987).
- [27] F. R. Husson and V. Luzzati *J. Phys. Chem.*, **68**, 3504 (1964).
- [28] R. Krishnaswamy, Ph.D Thesis: *Structure of Surfactant-Polyelectrolyte Complexes*, Jawaharlal Nehru University, New Delhi (2003).
- [29] I. Koltover, T. Salditt and C. R. Safinya *Biophys J.*, **77**, 915 (1999).

[30] P. Ileketi, L. Piculell, F. Tournilhac and B. Cabane *J. Phys. Chem*, **102**, 344 (1998).